Instrument Characterization for the Detection of Long-term Changes in Stratospheric Ozone: An Analysis of the SBUV/2 Radiometer

J. E. FREDERICK*

Laboratory for Atmospheres, Code 616, NASA/Goddard Space Flight Center, Greenbelt, MD 20771

R. P. CEBULA

SASC Technologies, Inc., Hyattsville, MD 27084

D. F. HEATH

Laboratory for Atmospheres, Code 616, NASA/Goddard Space Flight Center, Greenbelt, MD 20771

(Manuscript received 9 October 1985, in final form 18 February 1986)

ABSTRACT

The scientific objective of unambiguously detecting subtle global trends in upper stratospheric ozone requires that one maintain a thorough understanding of the satellite-based remote sensors intended for this task. The instrument now in use for long term ozone monitoring is the SBUV/2 being flown on NOAA operational satellites. A critical activity in the data interpretation involves separating small changes in measurement sensitivity from true atmospheric variability. This is the goal of the instrument characterization task, and of necessity it involves examining numerous details of SBUV/2 hardware operation. By defining the specific issues that must be addressed and presenting results derived early in the mission of the first SBUV/2 flight model, this work serves as a guide to the instrument investigations that are essential in the attempt to detect long-term changes in the ozone layer.

1. Introduction

The importance of implementing a program to detect long-term, global scale changes in the Earth's ozone layer has wide acceptance. In the 1970s, the period in which such a program was conceived, the only spaceborne remote sensor for ozone with a record of long-term performance was the Backscatter Ultraviolet Radiometer, first flown on the Nimbus-4 satellite in 1970. It was followed by the Solar Backscatter Ultraviolet (SBUV) Spectral Radiometer launched on Nimbus-7 in 1978 (Heath et al., 1975). Based on this history the long term ozone measurement program under the operational control of NOAA ulitizes an updated version of these backscatter instruments, denoted by SBUV/2. This paper focuses on the early in-orbit performance of the first of these sensors, SBUV/2 flight model 1, launched on the NOAA-9 operational spacecraft in December 1984.

An ozone measurement program must address three scientific concerns if it is to succeed in detecting long-term atmospheric change. These are 1) our present theoretical understanding of ozone variations, 2) limitations inherent in the measurement technique, and 3) characterization of hardware. Frederick and Serafino (1985) considered the first two of these topics in some detail. A major concern underlying stratospheric ozone measurements is the possibility of a long-term depletion associated with release of chlorofluorocarbons (CFC's). If a trend in ozone of the magnitude predicted by theory indeed exists, a viable measurement program should be capable of detecting this in a time period on the order of a decade. Central issues here involve a) the sensitivity of the SBUV measurable, backscattered radiance as a function of wavelength, to changes in ozone of the type predicted by theory and b) the possibility that background atmospheric variations can obscure the geophysical trend of interest. Frederick and Serafino (1985) showed that a depletion in ozone with an altitude dependence like that predicted for CFC's and a maximum trend of 4% per decade at 40 km would appear in the SBUV measurable as a wavelength dependent radiance increase with a maximum value of 1.6% per decade near 290 nm. Such a change is detectable by the SBUV technique provided the data set is essentially free of instrument drifts. Finally, Frederick and Serafino (1985) used the Nimbus-7 SBUV data set to estimate the magnitude of interannual variations in upper stratospheric ozone which could potentially obscure an underlying long-term trend. This indicated

* Present affiliation: Department of the Geophysical Sciences, The University of Chicago, Chicago, IL 60637.

that when the duration of the data set reaches one decade or longer, a trend like that predicted for CFC's is separable from background variations.

In a long-term measurement program a central issue involves the separation of subtle instrument artifacts from true atmospheric variations. This is the focus of the instrument characterization task, item 3 in the previous list. Such work obviously requires a thorough understanding of hardware performance as manifested by establishing quantitative relationships between instrument outputs and the atmospheric radiance. The objective of this paper is to define those aspects of in-flight hardware operation that influence the accuracy and stability of the in-orbit measurements made by the SBUV/2 flight model 1 launched on the NOAA-9 spacecraft in December 1984. The evaluation of instrument performance presented here utilizes data collected in the Activation and Evaluation (A and E) phase that took place after instrument turn-on in the period from January through March 1985. During this early portion of the mission the instrument operated in a series of modes designed to test all performance parameters necessary for successful routine operations. While a thorough understanding of these variables is necessary for evaluating the performance of the instrument over its scheduled two-year lifetime, the detection of any long-term atmospheric ozone trend ultimately requires piecing together data sets from several successive instruments. Of necessity, this activity cannot proceed in earnest for several years, the period required to collect a sizeable data set. It therefore becomes all the more important to thoroughly document the early in-orbit performance parameters of the first instrument since this information will be essential for analyses to be done many years after this writing.

2. Brief overview of the SBUV/2 instrument

This section briefly summarizes those aspects of the SBUV/2 sensor that must receive attention in the A and E analyses. No attempt is made to discuss the hardware in detail. A thorough description of the instrument has been given by Ball Aerospace Systems Division (1985) who designed and built the hardware, while Heath et al. (1975) have discussed a similar sensor flown on Nimbus-7.

The SBUV/2 instrument is a double grating monochromator capable of measuring absolute radiances over the wavelength range 160 to 405 nm with a 1.1 nm spectral resolution. The system also includes a coaligned cloudcover radiometer (CCR) centered on a wavelength of 379 nm with a 3 nm resolution. For Earth observations, the instrument field of view is directed downward and diffuse radiance backscattered by the Earth's atmosphere, surface, and clouds enters the monochromator. Three operating modes distinguished by the sequence of wavelengths observed are possible. In the "discrete mode" the instrument views 12 preselected wavelengths between 250 and 340 nm over a time period of 32 sec. This consists of 0.75 sec during which the gratings rotate to a know position followed by a 1.25 sec integration period. Grating position, the measure of wavelength, is indicated by either a primary or backup encoder. The signal, in counts per integration period from the SBUV/2 photomultiplier tube (PMT), corresponds to the 1.25 second time when the gratings are stationary. Eight seconds are required for the gratings to retrace to the starting position. Photomultiplier counts are output simultaneously on 3 gain ranges differing in sensitivity by factors of approximately 100 where range 1 is the most sensitive. Typical count rates lie between a zero offset and 2^{16}–1 per 1.25 sec integration period, although overflow values are allowed and appear as smaller count rates to which 2^{16}–1 must be added. Selection of the appropriate range for use in data processing is a software task. In the "sweep mode" the gratings step through the entire spectral range 405–160 nm where the wavelength interval betwen adjacent grating positions is approximately 0.074 nm. The PMT output in this mode corresponds to an integration over two grating positions totaling 0.1 sec. The total time required for one sweep of the spectrum and a grating retrace to the initial position is 192 sec. Finally, in the "position mode" the gratings remain stationary and the instrument observes a fixed wavelength signal until commanded to do otherwise.

For solar observations a reflecting diffuser plate is deployed in front of the instrument aperture at an angle of 28° below the horizontal. When the sun occupies the appropriate volume of space, the incoming solar beam strikes the plate and is reflected into the SBUV/2 entrance aperture as a diffuse radiance. Discrete, sweep, and position modes as described above are available for the solar measurements.

A frosted mercury lamp is attached to the inner side of the instrument aperture door and is viewed directly when the door is closed. Alternately, both the aperture door and the diffuser plate can be rotated so that mercury light reflected from the diffuser enters the instrument. This capability is used in the diffuser reflectivity measurement to be described in section 3. Finally, a chopper operating at a frequency of 20 Hz continually interrupts the radiance measurements to allow detection of any background signals, particularly contamination by energetic particles.

3. Instrument outputs related to geophysical quantities

This section presents the mathematical relationships between the desired geophysical quantities, being backscattered radiance $I(\lambda)$ and solar irradiance $F(\lambda)$ as functions of wavelength λ, and the outputs of the SBUV/2 instrument. These equations define the instrument parameters that must be examined to properly characterize the hardware. Put simply, the objective

of data analysis during the A and E phase of the mission is to ensure that the I, F, and λ values deduced from instrument outputs are as close to the true values as possible. The major outputs of concern here are 1) the count rate of the photomultiplier tube obtained in various instrument observing modes and 2) the position of the grating. With the count rate assumed to come from PMT gain range 1 and the instrument in the discrete Earth-observing mode, the backscattered radiance is given by

$$I(\lambda) = K_I(\lambda)[C(1) - C_0(1)] \quad (1)$$

where $C(1)$ is the PMT count rate in gain range 1 and $C_0(1)$ is the zero offset. The radiometric calibration constant for radiance at wavelength λ, $K_I(\lambda)$, is derived from preflight laboratory test data and here is expressed in the units radiance per count on PMT gain range 1. Ball Aerospace Systems Division (1985) presents a detailed discussion of the SBUV/2 radiometric calibration procedures used to derive $K_I(\lambda)$ including estimates of the uncertainties.

In practice, the signals from laboratory calibration lamps drive the instrument only onto gain range 1 or at most 2. Accurate ratios between the ranges are then required to obtain the instrument response to the much more intense signals observed in space. The SBUV/2 specification calls for a linear instrument response to within $\pm 1\%$ so that the calibration constants are nearly independent of count rate. The assumption of linearity is implicit in the mathematical development presented here, although as will be demonstrated, this represents an approximation to the instrument behavior observed in flight. When counts are taken from gain ranges 2 and 3, they must be converted to equivalent range 1 counts by use of the interrange ratio:

$$X_{1r} = \frac{C(1) - C_0(1)}{C(r) - C_0(r)} \quad (2)$$

where $r = 1, 2, 3$ indicates the range. Note that only a narrow range of count rates exists over which interrange ratios can be computed. In particular, when the signal on the less sensitive range reaches approximately 650 counts, the signal on the more sensitive range is near the $2^{16}-1$ maximum value. The general relationship between radiance and count rate on any gain range is then:

$$I(\lambda) = K_I(\lambda)X_{1r}[C(r) - C_0(r)]. \quad (3)$$

Derivation of the solar irradiance is more involved than (3) because of the diffuser plate used to convert the direct incident solar irradiance into a nearly isotropic radiance to which the instrument is intended to respond. To a first approximation the diffuser is a Lambertian surface whose reflectivity is independent of wavelength and the azimuthal angle of incidence, ϕ. The diffuse radiance reflected into the instrument aperture then varies as the cosine of the zenith angle of incidence, θ. Although reflectivity variations with wavelength and deviations from Lambertian behavior are minor, they must be included in the solar irradiance calculation. The major concern, however, is a possible long-term change in reflectivity resulting from exposure to the sun. In general, then, the reflectivity $R(\lambda, t, \theta, \phi)$ is a function of wavelength λ, time t, and the incident angles of the solar beam. The preflight irradiance calibration consists of directing a collimated beam of known irradiance onto the deployed diffuser plate at the fixed angles θ_c, ϕ_c and recording the PMT output. The laboratory calibration constant determined at an initial time t_c therefore includes $R(\lambda, t_c, \theta_c, \phi_c)$ implicitly. The relationship between solar irradiance $F(\lambda)$ and instrument response $C(r)$ on range r at any time t is

$$F(\lambda) = K_F(\lambda, t, \theta, \phi)X_{1r}[C(r) - C_0(r)] \quad (4)$$

where $K_F(\lambda, t, \theta, \phi)$ is the calibration constant including all angular dependence referenced to PMT gain range 1. This is related to the value $K_F^c(\lambda) \equiv K_F(\lambda, t_c, \theta_c, \phi_c)$ deduced preflight by

$$K_F(\lambda, t, \theta, \phi) = K_F^c(\lambda)\frac{R(\lambda, t_c, \theta_c, \phi_c)}{R(\lambda, t, \theta, \phi)}. \quad (5)$$

An important assumption enters at this point. As mentioned previously, the SBUV/2 instrument carries an onboard mercury calibration lamp to track temporal changes in the diffuser reflectivity, although this refers only to the fixed angles θ_{Hg}, ϕ_{Hg}, corresponding to near-normal incidence, at which lamp emission strikes the diffuser. Note that no information is available from these checks to define changes in the angular reflecting properties of the diffuser plate. The in-flight procedure implicitly assumes that the temporal and angular dependences of the reflectivity are separable. Mathematically this becomes

$$\frac{R(\lambda, t_c, \theta_c, \phi_c)}{R(\lambda, t, \theta, \phi)} = \frac{R(\lambda, t_c, \theta_{Hg}, \phi_{Hg})}{R(\lambda, t, \theta_{Hg}, \phi_{Hg})}\frac{R(\lambda, t_c, \theta_c, \phi_c)}{R(\lambda, t_c, \theta, \phi)} \quad (6)$$

where the first ratio on the right-hand side is assumed to account for all time dependence, and the second provides for a time independent angular response of the diffuser. Note that Eq. (6) constitutes an assumption and is not the result of a rigorous derivation. With the definition

$$\gamma(\lambda, \theta, \phi) = \frac{R(\lambda, t_c, \theta_c, \phi_c)}{R(\lambda, t_c, \theta, \phi)} \quad (7)$$

the final expression relating the solar irradiance to instrument response is

$$F(\lambda) = K_F^c(\lambda)\frac{R(\lambda, t_c, \theta_{Hg}, \phi_{Hg})}{R(\lambda, t, \theta_{Hg}, \phi_{Hg})} \times \gamma(\lambda, \theta, \phi)X_{1r}[C(r) - C_0(r)] \quad (8)$$

where $\gamma(\lambda, \theta, \phi)$ is measured preflight and the reflectivity is updated in orbit.

Degradation of the SBUV/2 optics and electronics over long periods in orbit will lead to a changing count rate for a given backscattered radiance or solar irradiance. Hence, the calibration constants K_I and K_F strictly apply only to the time of calibration. However, so long as the diffuser reflectivity and interrange ratios are properly evaluated, the quantity $I(\lambda)/F(\lambda)$ will remain unaltered by instrument drifts.

Finally, wavelength is determined from the expression:

$$\lambda = A \sin\alpha(g+\beta) \tag{9}$$

where g is the grating position indicator output by the primary or backup encoder and the argument of the sine function is in radians. The constants A, α and β are derived both pre- and postflight by recording the grating positions of known emission lines in the wavelength range 405 to 160 nm.

Equations (2), (3), (8), and (9) are the fundamental relationships that specify the quantities that must be known to evalute SBUV/2 in-orbit performance. These parameters are

a) The zero offsets, $C_0(r)$, in each of the three PMT gain ranges. These must include an analysis of possible spurious background signals arising from particle precipitation in the region of the South Atlantic magnetic anomaly.

b) The interrange ratios X_{1r}. In practice the derived quantities are X_{12} and X_{23} where $X_{13} = X_{12}X_{23}$.

c) The time dependent reflectivity of the onboard diffuser plate as deduced from the mercury calibration lamp.

d) The stability of the output of the mercury lamp over the time period required to measure the diffuser reflectivity.

e) The wavelength calibration of the instrument to ensure that the measured backscattered radiances and solar irradiances are assigned to the proper wavelength.

Sections 4–8 present the approach to determining each of the required quantities as well as results obtained during the A and E phase of SBUV/2 flight model 1.

4. Zero offset determination and contamination from the South Atlantic magnetic anomaly

On 11 January 1985, one day after turn-on of the SBUV/2 high voltage power supply, zero offsets were determined prior to opening the instrument aperture. A concern in accepting such early values as final ones stems from the fact that instrument electronics may not have stabilized in such a short time after high voltage turn-on. In the absence of additional measurements taken with the entrance aperture closed, 10 days of data collected in darkness with the solar zenith angle exceeding 120° were analyzed. The potential difficulty with this approach is that a small true signal might be present, although during the analysis the only additional source detected was from the moon. In one data set collected three nights away from the full moon, a zero offset for range 1 of 96.6 counts was derived, clearly showing contamination. This night's data were therefore excluded when deriving the final range 1 zero offset. No effect of scattered moonlight was visible in ranges 2 and 3 or in range 1 at times removed from the full moon.

A complication inherent in the zero offset determination concerns possible contamination from particle precipitation in the South Atlantic magnetic anomaly. The SBUV/2 signal chopper, similar to that described by Heath et al. (1975), is designed to detect such spurious signals and thereby allow their removal. To determine if energetic particle contamination appeared in the SBUV/2 outputs, data collected in the most intense region of the anomaly were examined and compared to values from areas free of particle precipitation. Contamination would manifest itself as an enhanced zero offset count in the nighttime measurements. Table 1 presents the final results. The zero offset derived for range 1 within the anomaly is slightly larger than that deduced elsewhere, although from the standpoint of practical applications the difference is insignificant. Note that the standard error derived for range 1 within the anomaly is substantially larger than that seen in regions that are free of particle precipitation. No effects from the South Atlantic anomaly appear in the mean zero offsets for SBUV/2 ranges 2 and 3 and the cloudcover radiometer (CCR).

5. Determination of interrange ratios

In a perfect photomultiplier tube, the interrange ratios X_{12} and X_{23} defined as

$$X_{ij} = \frac{C(i) - C_0(i)}{C(j) - C_0(j)} \tag{10}$$

for $(i, j) = (1, 2)$ and $(2, 3)$ would be constants independent of count rate and wavelength. This ideal case is not met by SBUV/2 flight model 1, although data collected on a routine basis still provide an adequate characterization of the required quantities. The following overview of PMT behavior allows one to anticipate the behavior displayed by the computed X_{12} and X_{23}. Currents corresponding to the count rates in gain range 3 are used for measuring the most intense signals, such as solar irradiance at wavelengths longer than 300 nm. This signal is drawn directly from the PMT cathode without amplification. Count rates for ranges 2 and 1 are used for weaker signals, with range 1 applying to the backscattered earth radiance at wavelengths less than 270 nm. Currents corresponding to ranges 2 and 1 are drawn from PMT dynodes after amplification. The cathode of the PMT is semitransparent, so that some fraction of the incident photons penetrate through the cathode and into the tube, with this fraction being wavelength dependent. One then

TABLE 1. Zero offsets and South Atlantic anomaly effects.

Range (r)	Outside anomaly		Inside anomaly		Mean of all data		
	$C_0(r)$	Std error	$C_0(r)$	Std error	$C_0(r)$	Std error	No. points
1	83.1	0.146	83.8	0.223	83.3	0.108	77,227*
2	65.4	0.005	65.4	0.004	65.4	0.003	85,560
3	59.6	0.028	59.5	0.021	59.5	0.013	85,560
CCR†	64.7	0.004	64.7	0.003	64.7	0.002	85,560

* Data points obtained within 3 days of the full moon were excluded in the range 1 calculation.
† Cloudcover radiometer.

expects the range 2 to range 3 ratio, X_{23}, to vary with wavelength. However, the range 1 to 2 ratio, X_{12}, should remain independent of wavelength. This reflects the fact that both the range 1 and range 2 currents are altered in the same way by the semitransparent cathode while the range 3 signal remains unaltered.

Two additional topics relevant to the SBUV/2 PMT performance are nonlinearity and time response where both of these anomalies could lead to a count rate dependence in the computed interrange ratios. Consider for example the range 1 to 2 ratio. If the PMT response on range 1 were exactly linear, then a doubling of the input radiance would be accompanied by a doubling in the count rate after correction for the background. However, if range 2 contained a slight nonlinearity, then the same doubling of input would lead to an output signal slightly different from twice the initial value. The exact change would depend on the magnitude of the count rate itself, leading to a count rate dependence in the computed X_{12} values. If, for example, the range 2 count rate increases more than linearly, one would expect X_{12} to decrease slightly as count rate increases. If range 3 were linear, then by Eq. (10) this same behavior would imply an increase in X_{23} with count rate.

The final concern is a longer than desired time response in the PMT. This simply means that when the input signal to the tube varies rapidly as the grating rotates to each new position, the current in the tube takes a finite time to adjust to its equilibrium value. The signal recorded during a 1.25 sec integration period at a fixed grating position will therefore not be the proper equilibrium current. The output signal here depends on the history of the input radiance over a period on the order of the PMT time constant. Such a problem would lead to different interrange ratios for solar irradiance and Earth radiance observations because of the very different time history of signal levels during these differing observing modes. As will be evident, all of the behaviors identified previously, being wavelength dependence, count rate dependence, and offsets between results for Sun and Earth observations, appear in the SBUV/2 interrange ratios.

A reliable absolute value of either the backscattered earth radiance or of the solar irradiance taken alone obviously requires accurate interrange ratios to extrapolate laboratory calibration constants derived on one PMT gain range to the gain range of the measurement made in orbit. However, for an atmospheric ozone derivation, the required quantity is the ratio $I(\lambda)/F(\lambda)$ as defined by Eqs. 3 and 8. In most cases $I(\lambda)$ is recorded on a different gain range than is $F(\lambda)$ and the ratio calculation requires that both quantities be referenced to a common scale. Therefore, it is not true that all factors related to instrument electronics cancel in the ratio of signals. An accurate instrument characterization is still required to derive accurate ratios of backscattered radiance to solar irradiance.

Figure 1 presents the interrange ratios X_{12} plotted against wavelength, and further divided according to count rate in range 2. The requirement for numerical evaluation of the interrange ratio is that the count rate on the less sensitive range (in this case, range 2) be sufficiently large as to be statistically meaningful after subtraction of the zero offset. We here sort $C(2)$ into the bins 400–500, 500–600, 600–700, and 700–800 counts. Figure 1 reveals a weak dependence of interrange ratio on count rate where X_{12} decreases slightly as the range 2 signal increases. A wavelength dependence also exists, where there is a small increase in X_{12} at wavelengths shortward of 300 nm. Based on the previous discussion it is not clear why X_{12} should show this behavior, although the unexpected variation with wavelength is small. For practical applications it is acceptable to take X_{12} to be constant and adopt a mean value over all count rates and wavelengths. Based on the data of Fig. 1, excluding count rates less than 500, this gives $X_{12} = 100.67$. Examination of results derived on a daily basis between days number 33 and 90 of 1985 showed no time dependence in X_{12}.

The range 2 to range 3 ratio can be derived from discrete Earth-viewing mode data for wavelengths of 305.6 nm and longer. At shorter Earth-viewing wavelengths the count rate on range 3 is less than 400, the minimum count rate that we consider in the calculations. All measurements from the discrete mode for the months of February and March 1985 were sorted according to count rate and wavelength. Figure 2 presents the results derived for March. The dependence of X_{23} on both count rate and wavelength is much more obvious than in the case of X_{12}. In particular, X_{23} is an increasing function of both variables, although the dependence on wavelength is the most pronounced. As

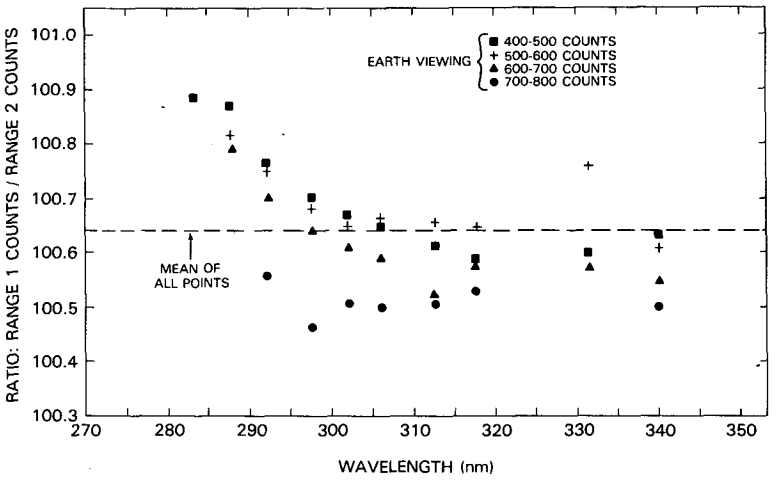

FIG. 1. The interrange ratio X_{12}, range 1 counts/range 2 counts, vs wavelength for several count rates on range 2.

an example, for range 3 count rates between 500 and 600, the value of X_{23} at 339.9 nm is 1.029 times that at 305.6 nm. The interrange ratio at all wavelengths increases by 1.6–1.7% as the count rate varies from 400–500 to 600–700.

The range 2 to range 3 ratio can also be derived from solar observations, and values at 273.5, 283.0 and 300 nm appear in Fig. 2. The dependence on wavelength is here essentially identical to that of the Earth-viewing mode. Note, however, that there is a shift between the X_{23} results derived from solar and Earth observations, with the solar values being slightly larger.

Finally, Fig. 3 presents the X_{23} values derived for the count rate interval $C(3) = 500$–600 at wavelengths 312.6 and 331.3 nm over the period from day number 33 to day 90 of 1985. A clear decrease exists over the period of observation and there is no indication that the trend has leveled off by the end of March. This reflects degradation in the PMT gain with time, a behavior that is not unusual. Therefore, the values in Figs. 1 and 2 should be taken as representative of March 1985 only. Evaluations and updates of the interrange ratios should be performed on a regular basis throughout the SBUV/2 mission.

6. Reflectivity of the onboard diffuser plate

It is clear from Eqs. (3) and (8) that the time dependent reflectivity of the SBUV/2 diffuser plate is a critical element in obtaining a stable set of $I(\lambda)/F(\lambda)$ values from which to derive atmospheric ozone profiles. If

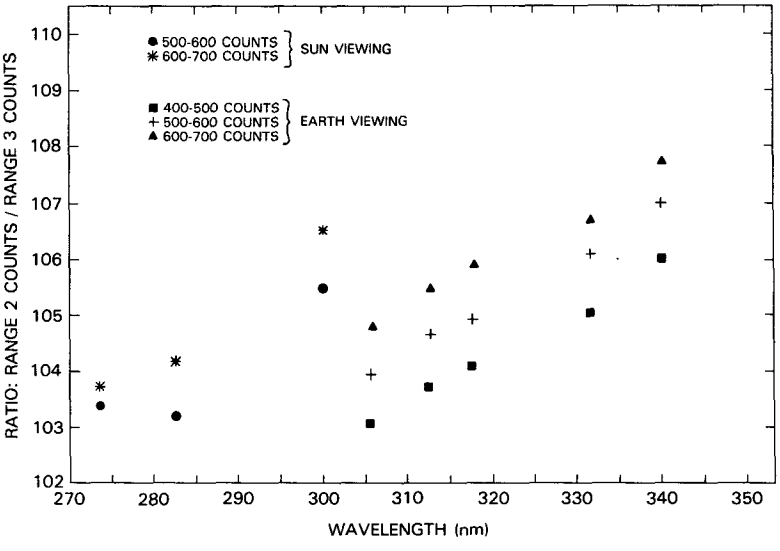

FIG. 2. The interrange ratio X_{23}, range 2 counts/range 3 counts, vs wavelength for several count rates on range 3. Values based on both discrete Earth-viewing data and solar data appear.

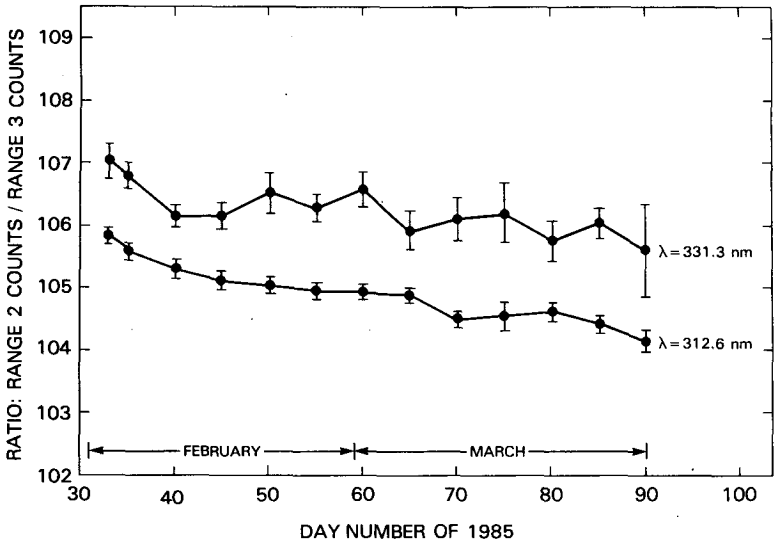

FIG. 3. Time dependence of the range 2 to range 3 count ratio, X_{23}, over the period February–March 1985. Values given for the wavelengths 312.6 and 331.3 nm.

one is to have the capability to distinguish changes of instrumental origin from true variability in the atmosphere, the reflectivity must be well characterized over the lifetime of the sensor. Values of $R(\lambda, t, \theta_{Hg}, \phi_{Hg})$ are determined by viewing in succession the frosted mercury lamp directly and the lamp signal reflected off the diffuser plate. The measurement sequence consists of ten scans performed using the sweep mode of the instrument where data from the first two scans are discarded to allow time for lamp warm-up. The remaining eight scans are taken such that two adjacent scans view the lamp emission reflected from the diffuser followed by two scans observing the lamp. The calculation utilizes data obtained at the ten most intense emission lines shown in the spectrum of Fig. 4. At their peaks these lines provide equivalent range 1 count rates of 2×10^4 per integration period or greater when viewing the lamp directly. The relative reflectivity is defined as

$$R(\lambda_{Hg}, t, \theta_{Hg}, \phi_{Hg}) = \frac{\int d\lambda [C_d(r) - C_0(r)]}{\int d\lambda [C_l(r) - C_0(r)]} \quad (11)$$

where the subscript d denotes a signal received from the diffuser and l indicates a direct view of the lamp. The wavelength λ_{Hg} refers to the center of a mercury emission, and the integrals are over the profile of each line. Numerical evaluation of Eq. 11 requires summing the count rates over a wavelength interval of approximately ± 1.0 nm, or 13–14 grating positions, on either side of each line center.

Figure 5 presents the relative diffuser reflectivities deduced preflight and during the A and E phase in February and March 1985. In flight, the orbit-to-orbit repeatability of the evaluation is good with the noise in the reflectivity result being roughly $\pm 0.5\%$. The mean values derived separately for February and March show no apparent changes in reflectivity over this time period.

7. Stability of the mercury calibration lamp

The onboard mercury lamp is the critical element used to track long term changes in the SBUV/2 wavelength calibration and, more importantly, in the reflectivity of the diffuser plate. In the latter evaluation it is essential that the output of the lamp remain stable over the time period required for a single diffuser calibration sequence, being 25 to 26 min. This ensures that the ratio of Eq. 11 is a measure of diffuser properties alone. The task is to determine the variation in count rate among the samples obtained for a given emission line during one diffuser reflectivity evaluation sequence. This procedure provides four count rates for

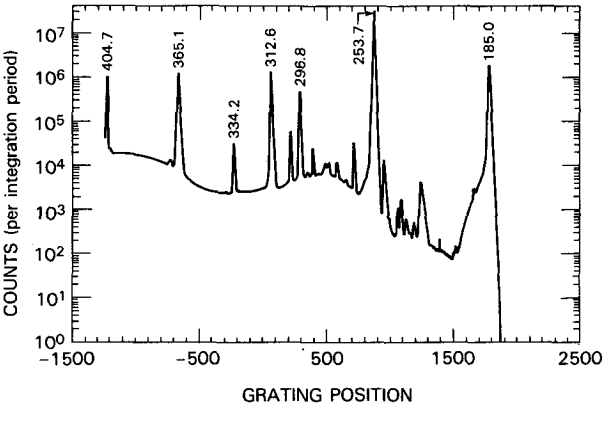

FIG. 4. Spectrum of the SBUV/2 mercury calibration lamp viewed directly.

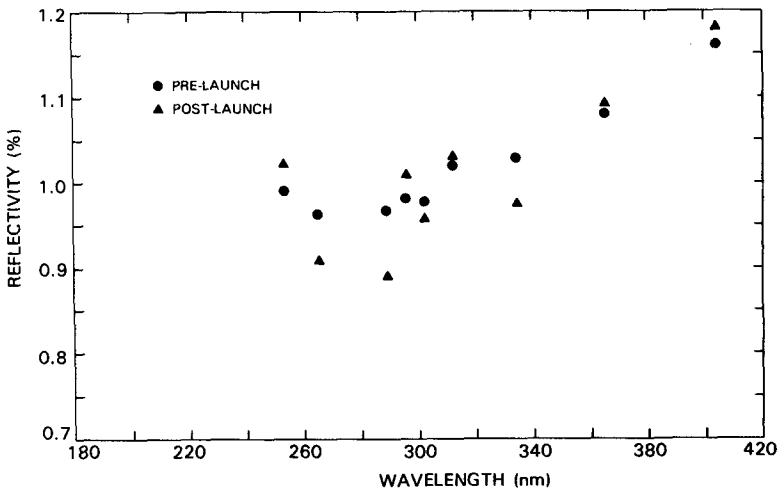

FIG. 5. Relative reflectivity of the SBUV/2 diffuser plate determined both preflight and early in the mission.

each line, both with and without the diffuser, for use in Eq. 11.

Table 2 illustrates the lamp stability at wavelengths of 253.7 and 404.7 nm for several reflectivity checks performed during the A and E phase. The reported quantities are ratios of maximum to minimum count rates obtained from observations of lamp emission in a fixed observing mode, being either a direct view of the lamp or of the diffuser. Ideally, the reported values would be identically equal to 1.0. The most obvious features in Table 2 are 1) the maximum to minimum ratios deviate most from unity when observing the mercury lamp directly, and 2) beginning with day number 79 of 1985 the output of the lamp became unstable. Prior to day 79, the lamp signal was constant to better than 1% while observing the diffuser, while the signal recorded when viewing the lamp directly was less stable, with maximum values as much as 3.6–3.7% above the minimum count rates. This behavior could arise from the fact that the lamp, when viewed directly, does not uniformly fill the SBUV/2 entrance aperture. Any small variation in the mercury arc position could then cause a fluctuation in the recorded signal. Such changes are washed out when the lamp emission is reflected from the diffuser and the signal uniformly illuminates the entire entrance aperture. On day 79, near the end of the A and E phase, a clear instability appears which, when observing the lamp at 404.7 nm, yielded maximum to minimum ratios in the range 1.11 to 1.19. The instability was less pronounced at 253.7 nm and in signals recorded while observing the diffuser, the ratio never reached 1.05 and dropped to lower levels after day 79. Figure 6 presents a time history of the absolute count rates for the 253.7 and 404.7 nm signals when viewing the lamp directly. Each point is the mean count rate obtained for a single line based on four spectral scans during one diffuser reflectivity evaluation sequence. The error bars represent one standard deviation, although for such a small sample these uncertainties do not have a rigorous statistical meaning. Rather, they serve only as a convenient measure of the instability. Long-term changes in lamp output are not a matter for concern so long as the mercury emissions are of sufficient intensity to be useful in the diffuser evaluations. However, a persistent short-term instability during the diffuser reflectivity measurements would pose a serious problem. Fortunately, data obtained subsequent to that in Fig. 6 reveal that the instability does not occur during every reflectivity evaluation sequence. Hence, the diffuser reflectivity evaluation can proceed so long as the data are properly screened.

TABLE 2. Stability of mercury lamp output over the course of a diffuser reflectivity measurement sequence.

	Observing diffuser		Observing Hg lamp	
Day (1985)	Count ratio max/min (253.7 nm)	Count ratio max/min (404.7 nm)	Count ratio max/min (253.7 nm)	Count ratio max/min (404.7 nm)
45	1.0043	1.0048	1.0145	1.0103
49	1.0032	1.0058	1.0122	1.0111
65	1.0060	1.0007	1.0368	1.0114
77	1.0090	1.0051	1.0356	1.0276
79	1.0439	1.0459	1.0784	1.1159
80	1.0111	1.0183	1.0431	1.1245
85	1.0196	1.0309	1.0543	1.1879

8. Wavelength calibration

The objective of onboard SBUV/2 wavelength calibrations is to detect any changes since the prelaunch tests and to allow for an accurate wavelength assignment to each grating position output by the instrument. Two operating modes are available for this. In the first,

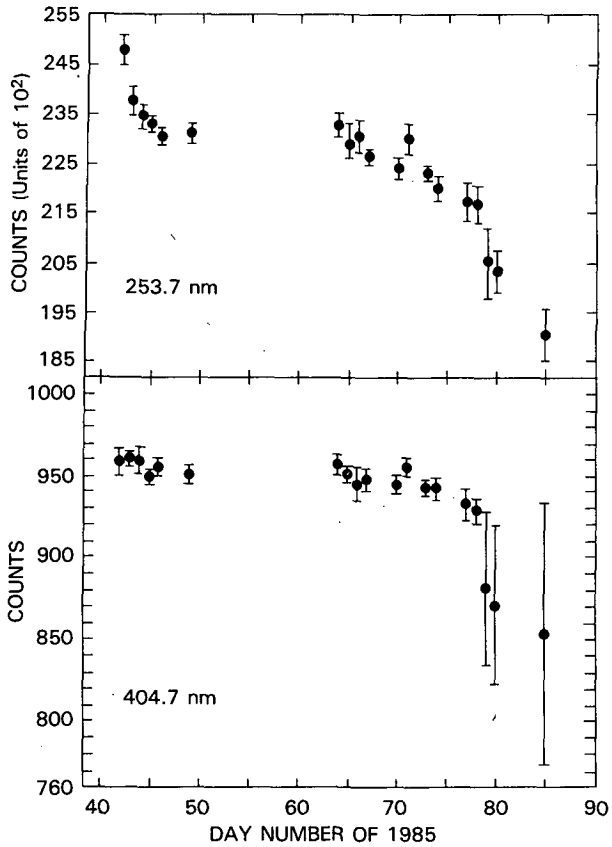

FIG. 6. Time history of PMT count rates recorded while observing the mercury lamp directly. Error bars represent one standard deviation and provide a measure of lamp instability. Note the discontinuity in the standard deviation on day 79.

referred to as the discrete wavelength calibration mode, the grating steps through 12 positions spaced across the 253.7 mercury emission line. In the second, the sweep mode calibration, the grating steps through its entire range while viewing the mercury lamp. Six Hg singlets in the spectrum between 185.0 and 404.7 nm are used here. Data for both sweep and discrete mode wavelength calibrations are obtained automatically as part of each diffuser reflectivity check. During in-flight wavelength calibrations in the sweep mode the approach is to determine the grating position g appropriate to the center of each mercury line. A fit to Eq. 9 yields the parameters A, α, and β which establish the wavelength of any grating position. An error analysis shows the uncertainty in the wavelength computed for a known grating position to be on the order of 10^{-4} nm. Comparison of calibrations performed before and after launch indicates no shifts in the grating positions of the mercury line peaks to within the accuracy of the procedure.

9. Discussion and conclusion

A critical issue in a program intended to detect long-term variations in atmospheric ozone involves developing and maintaining the ability to separate changes in the instruments over time from true changes in the atmosphere. Given the subtle way in which an ozone trend related to CFC chemistry should appear in a backscattered radiance data base, it is clear that the instrument characterization task must be an ongoing effort extending throughout the lifetime of each SBUV/2 sensor. In the search for long-term trends, stability of the data base over time is more important than absolute calibration. Since a new SBUV/2 instrument will be launched approximately every two years, it is likely that calibration biases will exist despite the detailed attention given to deriving the constants $K_I(\lambda)$ and $K_F(\lambda)$ in the laboratory. Once a long-term data base from several instruments exists, it will be sufficient to make a time independent adjustment in each individual SBUV/2 to place all results on a single absolute scale. This procedure presupposes that the results from each sensor are free of instrumental drifts. The attainment of this nearly drift-free ozone record is the responsibility of the instrument characterization task. The analysis presented here reveals several unexpected features in SBUV/2 performance, such as a wavelength dependence in the interrange ratios and an occasional instability in mercury lamp output. So long as these are accounted for in the processing, the search for long-term trends in ozone can proceed as the data set grows in duration.

This paper has outlined the issues that must be addressed in the analysis of outputs from the SBUV/2 instruments. Of necessity this study was restricted to the activation and evaluation phase of flight model 1, although the series of tasks outlined here can serve as a model for all subsequent characterization activities. In the future the two-year data base from each successive SBUV/2 instrument should be viewed as a whole, and all of the analyses described here performed using test data collected throughout the mission. It is only via such a meticulous process that we can attribute any changes observed in the measurements to true variations in atmospheric ozone.

Acknowledgments. The authors acknowledge Jean-Jacques Bedet for assistance in programming and data analysis. This work was supported by the National Aeronautics and Space Administration, Earth Science and Applications Division.

REFERENCES

Ball Aerospace Systems Division, *Specification Compliance and Calibration Data Book for SBUV/2 Flight Unit Number 1 (S/N 002), Volume II,* Document No. B6802-71, Boulder, Colorado, 1985. [Available from the Metsat Project Office, Code 480, NASA/Goddard Space Flight Center.]

Frederick, J. E., and G. N. Serafino, 1985: The detection of long term changes in stratospheric ozone: scientific requirements and current results from satellite-based measurement systems. *J. Climate Appl. Meteor.*, **24,** 904–914.

Heath, D. F., A. J. Krueger, H. A. Roeder and B. D. Henderson, 1975: The Solar Backscatter Ultraviolet and Total Ozone Mapping Spectrometer (SBUV/TOMS) for Nimbus-G. *Opt. Eng.*, **14,** 323–331.